Dual functionality metamaterial enables ultra-compact, highly sensitive uncooled infrared sensor

Jin Tao, Zhongzhu Liang, Guang Zeng, Dejia Meng, David R Smith, Qing Huo Liu, Qingrui Yang, Menglun Zhang, Wei Pang, Jingqiu Liang, et al.

Research article

Jin Tao, Zhongzhu Liang*, Guang Zeng, Dejia Meng, David R. Smith, Qing Huo Liu, Qingrui Yang, Menglun Zhang, Wei Pang, Jingqiu Liang and Tarik Bourouina*

Dual functionality metamaterial enables ultra-compact, highly sensitive uncooled infrared sensor

https://doi.org/10.1515/nanoph-2020-0607
Received November 11, 2020; accepted January 8, 2021; published online January 22, 2021

Abstract: Cointegration and coupling a perfect metamaterial absorber (PMA) together with a film bulk acoustic wave resonator (FBAR) in a monolithic fashion is introduced for the purpose of producing ultracompact uncooled infrared sensors of high sensitivity. An optimized ultrathin multilayer stack was implemented to realize the proposed device. It is experimentally demonstrated that the resonance frequency of the FBAR can be used efficiently as a sensor output as it downshifts linearly with the intensity of the incident infrared irradiation. The resulting sensor also achieves a high absorption of 88% for an infrared spectrum centered at a wavelength of 8.2 μm. The structure is compact and can be easily integrated on a CMOS-compatible chip since both the FBAR and PMA utilize and share the same stack of metal and dielectric layers.

Keywords: film bulk acoustic absorber; metamaterial; perfect material absorber; uncooled infrared detector.

1 Introduction

Uncooled infrared (IR) sensors are widely used in the fields of medical diagnostics, night vision, biological and chemical threat detection, electrical power system inspection, infrared spectroscopy, and thermal imaging. Their increasing impact is due to their compact size, low power consumption, and low cost. However, the wide dissemination of such infrared sensors is limited due to a lack of solutions for obtaining the multiple requirements of uncooling, wavelength-selectivity, high sensitivity, miniaturization and low-cost [1, 2].

FBARs, which feature a high temperature-sensitivity, must be seen here as an advantage since it can be applied to uncooled infrared sensors [3–6]. Indeed, upon infrared radiation, the temperature of the FBAR increases, while the resonance frequency decreases due to its negative temperature–frequency coefficient. The intensity of the incident infrared energy can then be retrieved from the frequency shift of the FBAR to realize the underlying sensing functionality. In this category of FBAR-based uncooled infrared detectors, Ang [4] developed an aluminum nitride (AlN) Lamb wave mode resonator and found that the sensing mechanism is based on both charge carrier generation and thermal effects. Xin [5] reported a resonant and resistive dual-mode resonator. Wang [6] used ZnO films and achieved a noise equivalent temperature difference (NETD) of 25 mK at 780 nm. They also found that lateral field excitation (LFE) FBAR exhibited a higher sensitivity in the infrared [7].

Jin Tao and Zhongzhu Liang have contributed equally to this work.

***Corresponding authors: Zhongzhu Liang**, State Key Laboratory of Applied Optics, Changchun Institute of Optics, Fine Mechanics and Physics, Chinese Academy of Sciences, Changchun, Jilin, 130033, China, E-mail: liangzz@ciomp.ac.cn; and **Tarik Bourouina**, State Key Laboratory of Applied Optics, Changchun Institute of Optics, Fine Mechanics and Physics, Chinese Academy of Sciences, Changchun, Jilin, 130033, China; and ESYCOM Lab, CNRS UMR 9007, University Gustave Eiffel, 77454 Marne-la-Vallée, France, E-mail: tarik.bourouina@esiee.fr. https://orcid.org/0000-0003-2342-7149
Jin Tao, Dejia Meng and Jingqiu Liang, State Key Laboratory of Applied Optics, Changchun Institute of Optics, Fine Mechanics and Physics, Chinese Academy of Sciences, Changchun, Jilin, 130033, China, E-mail: taojin@ciomp.ac.cn (J. Tao), djmeng@sklao.ac.cn (D. Meng), liangjq@ciomp.ac.cn (J. Liang)
Guang Zeng, Qingrui Yang, Menglun Zhang and Wei Pang, State Key Laboratory of Precision Measurement Technology and Instruments, School of Precision Instruments and Opto-Electronics Engineering, Tianjin University, No. 92 Weijin Road, Tianjin 300072, China, E-mail: guangzeng@tju.edu.cn (G. Zeng), yangqingrui@tju.edu.cn (Q. Yang), zml@tju.edu.cn (M. Zhang), weipang@tju.edu.cn (W. Pang)
David R. Smith, Center for Metamaterials and Integrated Plasmonics, Duke University, P.O. Box 90291, Durham, North Carolina 27708, USA; and Department of Electrical and Computer Engineering, Duke University, P.O. Box 90291, Durham, North Carolina 27708, USA, E-mail: drsmith@duke.edu
Qing Huo Liu, Department of Electrical and Computer Engineering, Duke University, P.O. Box 90291, Durham, North Carolina 27708, USA, E-mail: qhliu@duke.edu. https://orcid.org/0000-0001-5286-4423

It is worth mentioning that the absorption layer of those FBAR-based uncooled infrared sensors is usually composed of dielectric thin films of relatively low absorptions, only 17% for instance for Si_3N_4 [8]. Such low absorptivity only partially utilizes the full incident infrared energy, indicating that further optimization is needed. Therefore, the design and integration of an absorption layer appears as the key technology for FBAR-based uncooled infrared sensors. The traditional method of increasing the IR absorption is to add a lossy dielectric layer on top of the vibrating surface, which often increases the volume of the sensor, also increasing the response time and reducing the response sensitivity, leading to the deterioration of the overall device performance. It appears then necessary to develop higher absorptivity films that must be also ultrathin.

A perfect metamaterial absorber (PMA) is a synthetic periodic array made from subwavelength structures that can interact with incident light to produce a resonance [9, 10]. A PMA usually only absorbs a certain band of electromagnetic energy in either the visible, near infrared, terahertz or microwave regimes (theoretically approaching 100%) [11–15]. A PMA can be made from a multilayer structure consisting of a bottom metal film, a middle dielectric film and a top sub-wavelength structure. Near the resonant wavelength, the absorbed light is converted into thermal energy that changes the temperature of the device through Joule heating of the metal structure or from dielectric losses. Thus, PMA can be used in bolometers, thermal emitters, solar energy harvesters and others [16–22]. A plasmonic wave is generated in the near field due to the incident light coupling onto the surface. Localized surface plasmon resonance (LSPR) increases the intensity of the electric field at the close vicinity of the sub-wavelength structures, which greatly enhances the efficiency of light–matter interactions. This has already important applications in enhanced Raman scattering, sensing and detection [23–27]. The concept of PMAs was first proposed in 2008, and a peak absorbance greater than 88% was achieved at 11.5 GHz [9]. Then, a wide-angle, near-infrared-absorbing PMA was reported [17], where an incident angle of less than 80° allowed a 99% absorption over a narrow-band centered at 1.6 μm. Recently, a polarization-selective infrared sensor was realized using a two-dimensional asymmetric PMA [25]. PMAs have been widely used as absorbers in IR sensors and offer the advantages of being either polarization-sensitive [28] or -insensitive [29] and allowing wide incident angles [30, 31]. They can be either broad-spectrum [11, 32] or multi-wavelength absorption [33]. The greatest advantage of PMAs is that their thicknesses are much smaller than conventional electromagnetic absorbers (quarter wavelength). As a result, they have less impact on the sensor volume and related performance, which make them very suitable for sensor integration. In addition, the fabrication process of PMAs involves the deposition and etching of a metals or dielectric thin films, which is compatible with standard semiconductor processes. There are several studies on PMAs designed for the microwave, visible, near infrared and terahertz bands. However, there are very few reports on the integration of these absorbers with sensors in the long-wavelength, infrared, atmospheric window (8–14 μm).

In our work, an important novelty relates to the co-integration of both PMA and FBAR together—on top of each other and in the same chip. This is an important breakthrough, which has important consequences since it enables simple and low-cost fabrication of reliable uncooled infrared detectors. The cointegration also raised a counter-intuitive effect of coupling the FBAR with the PMA, which was found to improve the performance further. This paper proposes an uncooled, long-wavelength infrared ultra-compact sensor that combines PMA with FBAR, both cointegrated on the same chip, to eventually achieve high absorptivity and high sensitivity at a specific wavelength of 8.2 μm—chosen for demonstration of wavelength selectivity within the atmospheric window. In the proposed structure, the FBAR and PMA share the same metal and dielectric layers. Therefore, the overall thickness of the infrared sensor is greatly reduced, the degree of integration is improved, and the processing difficulty is reduced. This study helps solving the contradictory requirements fort high absorptivity and high sensitivity of uncooled infrared sensors, and provides a reference for the cointegration of micro–nano-scale plasmonic PMA onto FBAR structures within CMOS-compatible chips to achieve high-performance infrared devices, in particular the uncooled infrared sensors under consideration in this work.

2 Results

2.1 Design and fabrication

The proposed infrared sensor is the cointegration result of an FBAR and a PMA, both sharing the same multilayered thin-film stack, as illustrated in Figure 1a. The FBAR is composed of an aluminum nitride (AlN) piezoelectric film sandwiched between two metal electrodes (Mo). The total thickness of the FBAR is ~1.5 μm and the area is ~15,000 μm^2. The FBAR couples electrical energy into mechanical energy and vice versa thanks to the

piezoelectric nature of the AlN layer. An AlN thin film was used here as the dielectric layer in the PMA for two reasons. First, the AlN film has a good process compatibility with other thin film materials. Second, the AlN film has a larger dielectric constant, indicating that a smaller film thickness is required. In addition, the thin infrared absorption layer has little effect on the performance of the FBAR, which provides a high device sensitivity, reduces the heat capacity and improves the response rate. The device structure proposed in this paper combines the advantages of the PMA's high absorptivity with the FBAR's high sensitivity, and has the advantages of being highly integrable with existing fabrication methods and having a simple fabrication process. An AC signal is connected to the electrodes to drive the FBAR at its first natural mechanical resonance frequency. The fundamental eigen-frequency of the FBAR in thickness-stretch mode is determined by the properties of the piezoelectric film, and can be simply expressed as $f_s = V_s/2d$, where V_s and d are the acoustic velocity of compressional waves at resonance and thickness of the piezoelectric layer, respectively. V_s is governed by the Young's modulus E and density ρ of the piezoelectric material as $V_s = \sqrt{E/\rho}$. As the temperature changes, predominantly due to the absorbed infrared light, both E and ρ vary, leading to changes in V_s. In turn, these changes cause the resonance frequency of the FBAR to shift, as illustrated in Figure 1a. FBARs are indeed known to be temperature-sensitive and have previously been used in temperature-sensing applications [7] and this is taken here as an advantage to measure infrared radiation through the induced heating of the absorber. As can be seen in Figure 1a, due to its piezoelectric nature, the FBAR exhibits actually two characteristic frequencies f_s and f_p, called resonance and antiresonance, respectively. It is worth-mentioning that the resonance occurs at f_s as it corresponds in this representation to minimum impedance, also corresponding to maximum vibration amplitude. The two frequencies closely linked to each-other through the electromechanical coupling coefficient (k_t^2) with $f_s = f_p\,(1 - 4k_t^2/\pi^2)$ [34].

The PMA results from the combination of the top molybdenum electrode of the FBAR together with the golden metal array, being separated by an AlN dielectric layer, as illustrated in Figure 1a. AlN was used here as the dielectric layer for two reasons. The first is the high dielectric constant of AlN, resulting in a thinner film. The second is the feasibility of the fabrication process. The thickness of the AlN dielectric layer is ~200 nm, the pitch of the metal array is 3 μm, and the gap between two square metal plates is 1 μm. When electromagnetic (EM) waves impact the PMA at normal incidence, the corresponding specific wavelength couples with the PMA. EM energy is absorbed by the PMA and converted into thermal energy. This thermal energy heats the FBAR, causing the frequency shift shown in Figure 1b. An scanning electron microscope (SEM) image of the proposed device is shown in Figure 1c. The inset view shows the cross-section of the FBAR and the metal array (a = 2 μm, b = 1 μm). The top surface of the FBAR is exposed to air and the bottom surface is isolated from the substrate by a cavity to prevent the leakage of resonant mechanical energy. More details on the design are presented in Supplementary material (section 2)

A high-quality uniform AlN piezoelectric layer was deposited by a low-temperature (~250 °C) sputtering process. The metal array of the PMA was patterned by electron beam lithography (EBL). Considering the sizes and accuracy, it could also be patterned by UV lithography. Thus, the fabrication process is integrable and CMOS-compatible, which is a key factor in the practical applications of the proposed sensor across various fields.

2.2 Characterization

The frequency response of the FBAR was measured using a Vector Network Analyzer, and it is shown in Figure 2a. The black line shows the response of the bare FBAR without the metal array, and the red line shows the response of the FBAR after the metal array has been deposited on the surface. In the latter case, f_p decreased because of the added metallic array. f_p became closer to f_s whose position did not change. This means that the electromechanical coupling coefficient (k_t^2) also decreased. The results also show that the Q factor increased at f_s (Q_s) and decreased at f_p (Q_p). The resonant mode of the bare FBAR is uniform in the thickness direction. After adding the metal array, the paths of acoustic waves beneath the metal pads and gaps are different, and the resonant mode splits into two distinct forms as can be seen from Figure 2a which reveals the appearance of a second small dip at a frequency below f_s. This dip corresponds to an increased apparent thickness (see also Figure S3b in Supplementary material). Hence the metal array causes the dispersion of resonant energy, and in turn, it contributes to the decrease of k_t^2 [35]. At the frequency f_p, acoustic wave scattering is enhanced near the interface between the FBAR surface and the added metal array, which causes a decrease of Q_p. At the same time, the metal array restricts the area of propagation and leakage of the transverse waves propagating at the frequency f_s, leading to an increase of Q_s. Thus, the slope of the impedance–frequency curve increases, which indicates the increasing sensitivity of the sensor

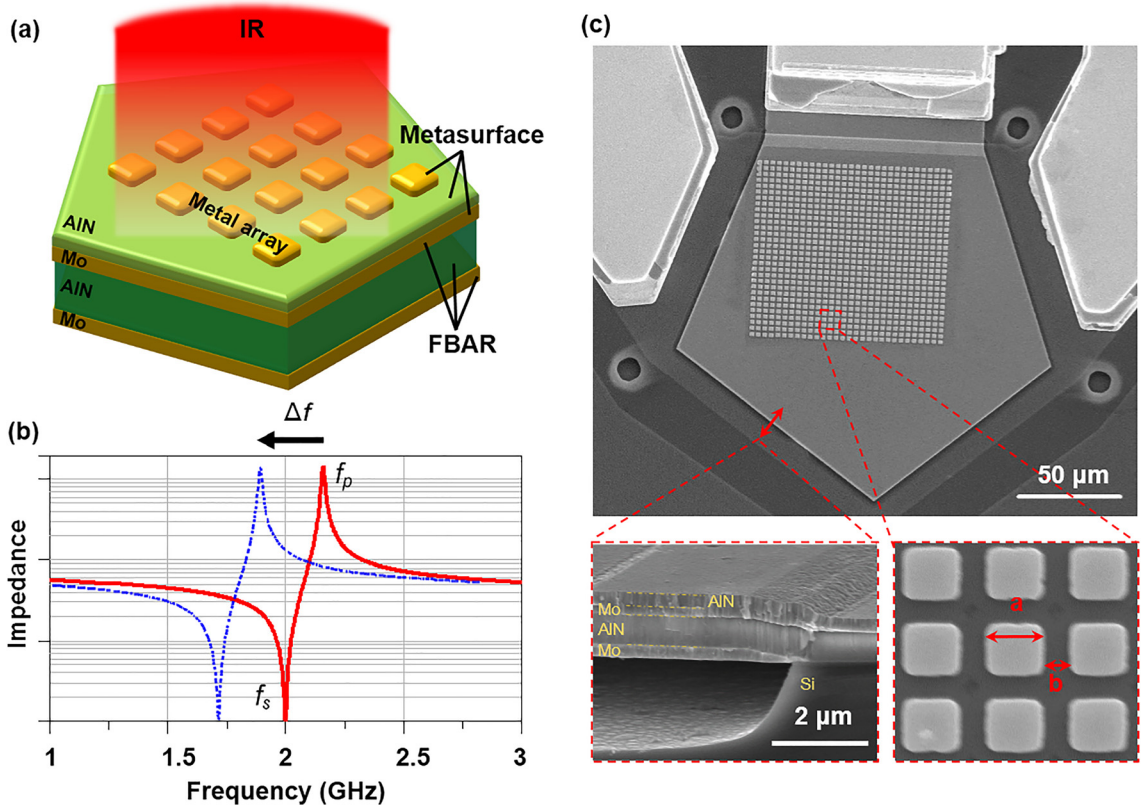

Figure 1: (a) Schematic layout of the proposed sensor. (b) Temperature-induced resonance frequency shifts down upon infrared (IR) irradiation. (c) Scanning electron microscope (SEM) image of the proposed sensor, cross-section of film bulk acoustic wave resonator (FBAR), and metal array of square plates. The length a of each square is ~2 μm and the gap spacing b between two neighboring squares is ~1 μm.

operating at f_s. The calculations of Q, k_t^2 and more details about the FBAR can be found in Supplementary material (section 4).

By measuring the frequency responses at different temperatures, the temperature coefficient of frequency (TCF) of the proposed sensor was found to be –53.75 kHz/°C (–23 ppm/K), as shown in Figure 2b and c. TCF is usually an intrinsic property of materials that is dependent on the growth conditions. The TCF of the proposed device is comparable with previously reported values [3, 5, 36]. Figure 2c also shows that the proposed sensor has a large linear dynamic range, which is beneficial for practical applications.

The IR absorption spectrum, measured by Fourier transform infrared (FTIR) microscopy, is shown in Figure 2d. More details on the corresponding experimental setup are presented in Supplementary material (section 5). The red and black lines represent the IR absorption of the perfect metamaterial absorber and AlN surface (surface of bare FBAR), respectively. Strong absorption can be observed around a wavelength of 8.2 μm, with the maximum absorption of 88%. The absorption of the AlN surface without the PMA is only about 14%. Thus, the perfect metamaterial absorber causes a 6× enhancement in IR absorption. Absorption is directly related to the responsivity, noise equivalent power (NEP), NETD, and detectivity of the IR sensor. Therefore, an increase in absorption also improves the performance of the IR sensor. There are small peaks at a wavelength of 11.3 μm (888 cm^{-1}) for both the AlN surface and PMA, corresponding to the intrinsic absorption peak of the AlN material [37].

In the design phase, we simulated the PMA using a commercial finite difference time domain (FDTD) solver to identify the optimal structure. The periodic unit cell is shown in Figure 3a. We used AlN as the dielectric spacer and simulated the dielectric constant as in literature study [38]. The metal array was modeled as a pattern of gold using a Drude model with a plasma frequency of $\omega_p = 2\pi \times 2175$ THz and collision frequency of $\omega_c = 2\pi \times 6.5$ THz [39]. The reflective plane was taken to be Mo [40]. The transmission T and reflection R were obtained from S-parameter simulations with appropriate boundary conditions to approximate a transverse EM wave incident on the structure. Because of the thick reflective metal plane, T was zero. The absorption

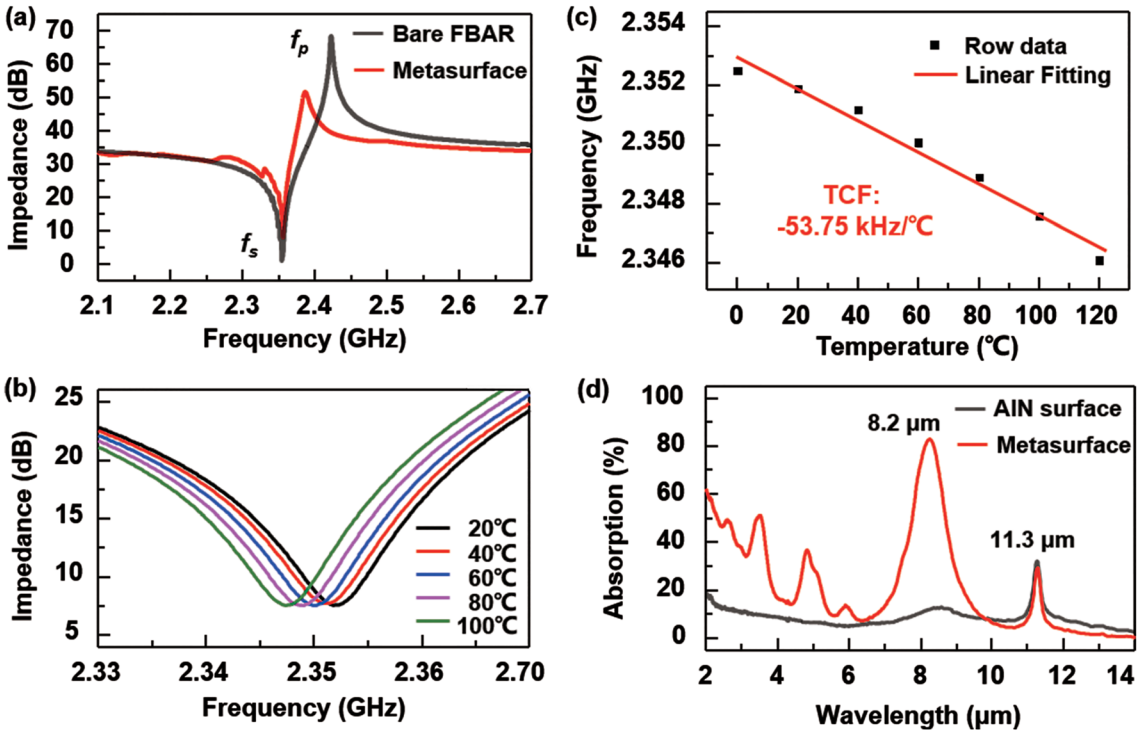

Figure 2: (a) Frequency response of the film bulk acoustic wave resonator (FBAR) with perfect metamaterial absorber (PMA) (red line) and without PMA (black line). (b) Frequency responses of the proposed sensor recorded at temperatures from 20 to 100 °C. (c) Temperature coefficient of frequency (TCF) also referred to as temperature responsivity (R_{ts}) of the proposed sensor was evaluated from measurements as –53.75 kHz/°C (–23 ppm/K). (d) Infrared (IR) absorption of perfect metamaterial absorber (red line) and AlN surface (black line) measured by Fourier transform infrared (FTIR) microscopy.

was then calculated as $A = 1 - R$. The simulation results for the frequency-dependent absorption are shown in Figure 3b, where the center frequency is 8.3 μm and the maximum absorption rate is 96%. The measurement results show a center frequency of 8.2 μm and a maximum absorption rate of 88%. This slight mismatch may be caused by the tolerance levels inherent to the fabrication process.

To understand the resonance mode in the absorption band, the EM field distribution at 8.3 μm was simulated; the results are shown in Figure 3c and d, which show the distribution of the dominant components H_y and E_x, respectively. It can be seen that the magnetic resonance is strongly excited, and this could interact and couple with the magnetic field of the incident light [41]. Therefore, a strong enhancement in absorption resulting from surface plasmonic resonance is achieved between the top and bottom metal layers around the resonance frequency. The absorbed EM energy is converted to heat and transferred to the underlying FBAR, raising its temperature.

The response of the fabricated IR sensor was characterized using a Globar as an IR source. The sensitivity and dynamic range of the IR sensor were measured by changing the power of the incident IR radiation, as shown in Figure 4a. The IR response of the device was measured at 10.6, 14.5, 31.8 and 58.0 μW/mm^2, causing frequency shifts of –14, –20.5, –44.5 and –96 kHz, respectively. The responsivity was then evaluated to be 1.65 kHz/(μW/mm^2), as shown in Figure 4b. The responsivity can also be expressed as 110 Hz/nW over the sensing area of 15,000 μm^2. This result indicates a much higher sensitivity than those of previous reports [3, 5]. The results also exhibit good linearity and a large dynamic range.

For the sake of comparison, the incident IR was also detected using a conventional FBAR without the perfect metamaterial absorber. The results are shown in Figure 5. The frequency shift of the bare FBAR and the proposed device was measured at the same IR exposure. The frequency shift of the FBAR was –65 kHz on exposure to 58 μW/mm^2 IR irradiation, whereas that of the proposed sensor was –96 kHz, indicating a ~1.5× enhancement. Although the maximum absorption of the PMA was about 88%, which is almost 6× that of the AlN surface (see Figure 2d), this was for a rather narrow spectrum at resonance. It is worth mentioning that our measurements shown in Figures 4 and 5 used broadband (1 μm) incident

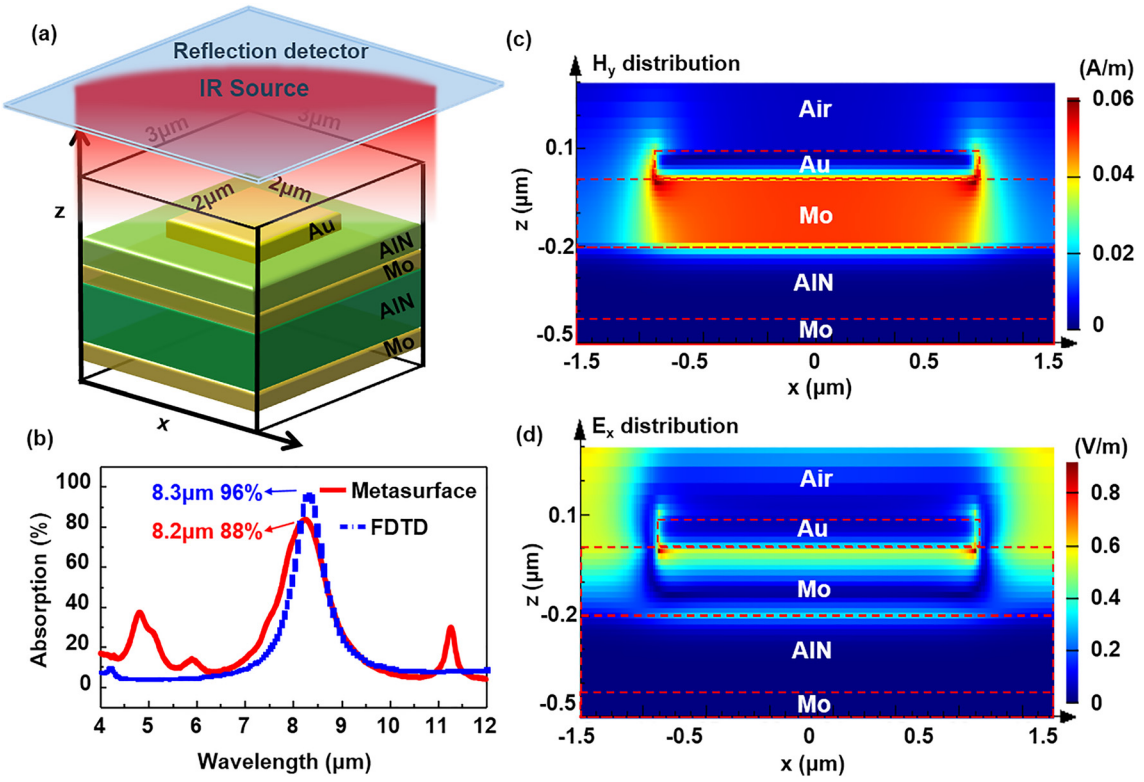

Figure 3: (a) Schematic of the periodic unit cell of the perfect metamaterial absorber. (b) Simulated (blue dashed line) and measured (red solid line) infrared (IR) absorption spectra of the perfect metamaterial absorber. (c) Magnetic field (H_y component) distribution at a wavelength of 8.3 μm. (d) Electric field (E_x component) distribution.

IR, so the average enhancement does not reach the maximum factor of six. In Figure 5, we can also observe a significant difference in the time responses. The thermal response of the proposed sensor is merely 25 s, that is much slower than for a bare FBAR. The dimensions of a bare FBAR is only 0.7 mm × 0.7 mm × 0.4 mm while those of our sensor cointegrating both the FBAR and the PMA, are 10 mm × 10 mm × 0.4 mm. The bigger volume has a bigger thermal capacity, although combined with an increased heat transfer rate with the surrounding environment due to the increased surface area, both effects eventually leading to a larger thermal time constant due to the increased volume-to-surface ratio. According to scaling laws, it is expected that reducing the device size further would reduce the time constant.

NEP is a crucial parameter in IR sensors, and is defined as the frequency noise spectral density $\langle f_n \rangle$ divided by the responsivity (R_s) of the sensor, that is NEP = $\langle f_n \rangle / R_s$. The value of R_s = 100 Hz/nW is taken from the result shown in Figure 4b, while the value of $\langle f_n \rangle \sim 21.2$ Hz/Hz$^{1/2}$ was extracted from measurements of the short-term frequency stability (see Supplementary material—section 6). We finally obtain NEP = 0.2 nW/Hz$^{1/2}$. Furthermore, the specific detectivity D^* is also evaluated using the equation, $D^* = \sqrt{A}/\text{NEP}$, where A = 15,000 μm^2 is the area of the proposed sensor. It is found to be $D^* = 6 \times 10^7$ cm$\sqrt{\text{Hz}}$/W, which is considered as a rather low value especially when compared to those of other cooled photodetectors, which can be two or three orders of magnitude larger.

However, when considering thermal imaging application, NETD is among the most relevant figures of merit. It quantifies the temperature change of a scene, which is required to produce a signal equal to the RMS noise. Small values of NETD allows obtaining a better contrast for distinguishing and object whose apparent temperature is very small compared to the temperature of the background. According to the method described by Shang et al. [42], NETD can be evaluated from the noise-induced frequency fluctuation $\langle f_n \rangle \sqrt{\Delta f}$ divided by the temperature responsivity R_{ts}, that is NETD = $\langle f_n \rangle \sqrt{\Delta f}/R_{ts}$, where in our case, Δf = 200 Hz is the measurement bandwidth and R_{ts} = 53.75 kHz/°C taken from the result shown in Figure 2c. NETD is then evaluated as 5.5 mK. Even though the detectivity D^* is not very high, the very low NETD value reached in this work could be due to the fact that our detector has a frequency output (while most detectors has either a current or a voltage output) whose good stability is combined with a high thermal responsivity. Another

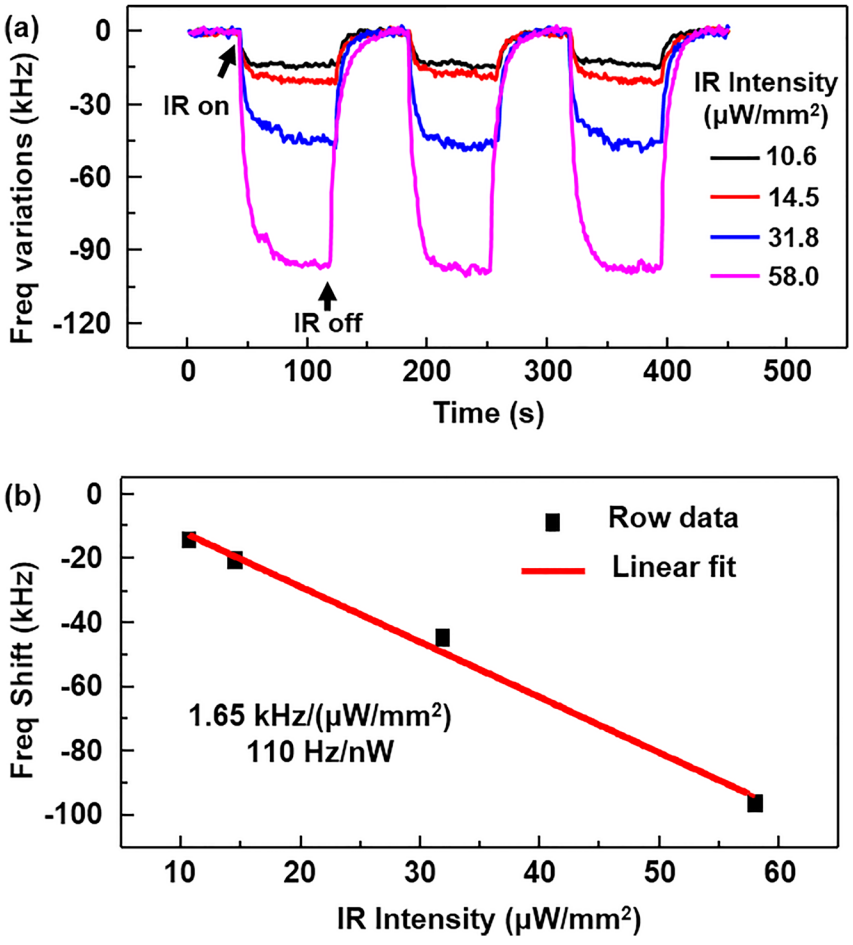

Figure 4: (a) Frequency response to different infrared (IR) intensities. (b) Responsivity of the proposed sensor with a sensing area of 15,000 μm^2 is evaluated to be 1.65 kHz/(μW/mm^2), also equivalent to 100 Hz/nW.

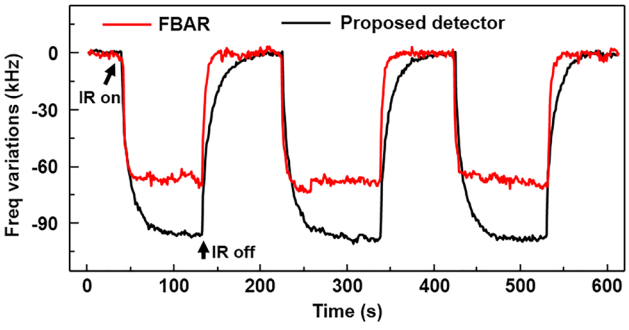

Figure 5: Measured response of the proposed sensor and a bare film bulk acoustic wave resonator (FBAR) to modulated infrared (IR) radiation (58 μW/mm^2). The proposed sensor shows 1.5× enhanced responsivity.

possible reason is that NETD is not directly dependent on surface area A, while D^* is. This value of 5.5 mK for the NETD appears as an excellent value among uncooled photodetectors and it is also comparable to the best NETD of cooled infrared detectors (see Supplementary material —section 1).

3 Discussion

Usually, an FBAR consists of three layers (Mo–AlN–Mo). In practice, a passivation layer of AlN is added to the surface of the FBAR to protect the top Mo electrode from oxidation, thus forming a four-layer structure (Mo–AlN–Mo–AlN). A perfect metamaterial absorber also usually consists of three layers (metal–dielectric–metal). In our device, the above-mentioned passivation layer (AlN) can function as the dielectric layer of the PMA while the top electrode (Mo) of the FBAR functions as the metal reflective layer. Thus, the fabrication of the proposed IR sensor is quite simple, requiring only the addition of a single layer of patterned gold acting as a plasmonic metallic array on top of the FBAR. This simple structure ensures reliability, low cost, and integrable fabrication. Nowadays, FBARs are commercially available and their fabrication process is quite mature, which makes the proposed sensor one of the most promising candidates for the realization of next-generation miniaturized, low-cost, low-power, and high-performance uncooled IR sensors.

Even though the proposed sensor possesses a unique combination of high responsivity, high IR absorption, a simple and compact structure, and CMOS compatibility, there is still plenty of room to improve the performance of the FBAR-based IR sensor. First, efficient thermal isolation anchors could be employed to reduce the thermal conduction loss, thereby improving the responsivity of the sensor. Such anchors can also be designed so as to provide further mechanical decoupling, leading to a reduction of resonant mechanical energy loss to the substrate. In the proposed device, the bottom electrode is connected to a silicon substrate and the piezoelectric layer continues along the substrate. These two structures result in significant heat loss. For structural optimization, the thermal conductivity should be decreased. For the same IR radiation, the device will then record a higher temperature and a larger frequency shift. Second, the perfect metamaterial absorber does not cover the full surface of the FBAR, as shown in Figure 1c. If the entire surface of the FBAR was covered by the PMA, the total amount of IR radiation would increase, resulting in higher IR absorption. Moreover, thanks to the easy cointegration of PMA together with the FBAR, the proposed device can be thinner, leading to higher resonant frequency and smaller thermal capacity, both of which contributing to higher responsivity of the IR sensor. Third, the area of the proposed sensor could be further reduced to less than $20 \times 20\ \mu m^2$ (the size of common commercial uncooled IR sensors), and the device could be fabricated in arrays for use in IR imaging systems. Finally, the resonance frequency of the FBAR could be increased to, say, 10 GHz to achieve higher sensitivity in the sensor. At the same time, the thickness of the FBAR would be thinner, reducing further the heat capacity of the sensor.

The dynamic range of the sensor can be discussed based on the results shown in Figures 2 and 4. On one hand, Figure 2(b) and (c) is the experimental data showing that the proposed device can work in the temperature range from 0 to 120 °C and that within this range, there is a linear response of the sensor's frequency as a function of temperature. To the best of our knowledge, other infrared detectors/sensors can difficultly behave in a similar manner. Higher temperatures than 120 °C have not yet explored yet on our sensor. One can expect that within certain temperature limits, nonlinear behavior may occur, in particular when reaching irreversible thermomechanical effects.

On the other hand, Figure 4(b) shows the frequency shift versus the incident intensity of infrared light. An incident power density of $58.0\ \mu W/mm^2$ causes a frequency shift of –96 kHz. The corresponding temperature variation of the device can be evaluated as 1.78 °C, considering that the temperature coefficient of frequency (TCF) was found to be –53.75 kHz/°C. Then, according to the linear response shown in Figure 2c, our device should be able to sustain at least a power density of $3258\ \mu W/mm^2$ corresponding to the maximum temperature of 120 °C considered in our investigations.

It is also worth mentioning that when considered as a stand-alone device, it is impossible for the proposed detector to distinguish between the temperature change of its environment and the temperature change caused by the IR irradiation. Usually, two ways can prevent the temperature interference. First, a thermo electric cooler is used to stabilize the working temperature of the IR detector. Second, a reference IR detector, which is shielded from the IR irradiation, is encapsulated in the same package together with the IR detector which is exposed to the IR irradiation. A differential operation of the two signals can eliminate the effect of the environmental temperature.

4 Conclusion

In conclusion, we have demonstrated an uncooled IR sensor based on an FBAR and a perfect metamaterial absorber. The high IR absorption of the perfect metamaterial absorber (88% at around 8.2 μm) enhances the responsivity of the proposed sensor by 50%. It is worth mentioning that this 1.5 times (50%) enhancement is achieved within a rather broadband IR illumination from 7.5 to 8.5 μm—keeping in mind that the only spectral range of interest is 8–14 μm. However, by looking at Figure 2(d), a rough estimation of the averaged improvement of absorption near 8 μm (±0.5 μm) is somewhere between 200 and 300%; the discrepancy with the observed 50% enhancement in the responsivity is possibly due to the counter-effect of the enlarged effective heat capacity of the PMA, which required adding alumina and gold layers on top of the FBAR, but this statement requires more investigations. When considering a narrower bandwidth around 8.2 μm, the predicted enhancement is merely six times (500%). In our experiments shown in Figure 2, the IR absorption at 8.2 μm is 0.88 for PMA compared to 0.15 for a simple AlN surface, that is a 6× improvement. The PMA and FBAR share the same metal and dielectric layers to form a compact and robust stack that converts IR irradiation to heat with high efficiency. The temperature-sensitive properties of FBARs allow the proposed IR sensor to achieve high sensitivity ($1.65\ kHz/(\mu W/mm^2)$) and high resolution (NEP ~ $0.2\ nW/Hz^{1/2}$ and NETD ~ 5.5 mK). Therefore, the proposed sensor appears to exhibit several advantages, such as a compactness, high sensitivity, high

resolution, low power consumption, as well as CMOS-compatibility, making it a promising candidate for next generation high-performance uncooled IR sensors.

5 Experimental section

Fabrication: Details are given in Section 3 of Supplementary material.
Measurements: Details are given in Sections 5 and 6 of Supplementary material.

Acknowledgements: We thank Dr. Alexandre Baron, Dr. Xiaojun Liu in Duke for useful discussion.
Author contributions: All the authors have accepted responsibility for the entire content of this submitted manuscript and approved submission.
Research funding: This work is supported by the National Natural Science Foundation of China (Grant Nos. 61735018, 61376122 and 61805242), Excellent Member of Youth Innovation Promotion Association CAS (Grant Nos. Y201836, 2014193), Scientific and Technological Development Project of Jilin Province (Grant Nos. 20170204077GX, 20190103014JH), Leading Talents and Team Project of Scientific and Technological Innovation for Young and Middle-aged Groups in Jilin Province (Grant No. 20190101012JH), CAS President's International Fellowship Initiative (PIFI), Independent fund of State Key Laboratory of Applied Optics, Overseas Students Science and Technology Innovation and Entrepreneurship Projects, Project of CIOMP-Duke Collaborative Research, Project of CIOMP-Fudan University Collaborative Research.
Conflict of interest statement: The authors declare no conflicts of interest regarding this article.

References

[1] A. Rogalski, P. Martyniuk, and M. Kopytko, "Challenges of small-pixel infrared detectors: a review," *Rep. Prog. Phys.*, vol. 79, p. 046501, 2016.
[2] A. Rogalski, "Recent progress in infrared detector technologies," *Infrared Phys. Technol.*, vol. 54, pp. 136–154, 2011.
[3] Y. Hui, J. S. Gomez-Diaz, Z. Qian, A. Alù, and M. Rinaldi, "Plasmonic piezoelectric nanomechanical resonator for spectrally selective infrared sensing," *Nat. Commun.*, vol. 7, p. 11249, 2016.
[4] W. C. Ang, P. Kropelnicki, Y. Zhu, et al., "Uncooled resonant infrared detector based on aluminum nitride piezoelectric film through charge generations and lattice absorptions," *Appl. Phys. Lett.*, vol. 104, p. 201110, 2014.
[5] X. Li, J. Liang, H. Zhang, et al., "Resonant and resistive dual-mode uncooled infrared detectors toward expanded dynamic range and high linearity," *Appl. Phys. Lett.*, vol. 110, p. 263502, 2017.
[6] Z. Wang, X. Qiu, J. Oiler, J. Zhu, and H. Yu, "Film bulk acoustic-wave resonator (FBAR) based infrared sensor," in *2010 IEEE 5th Int. Conf. Nano/Micro Eng. Mol. Syst., Xiamen*, 2010, pp. 824–827.
[7] Z. Wang, X. Qiu, S. J. Chen, et al., "ZnO based film bulk acoustic resonator as infrared sensor," *Thin Solid Films*, vol. 519, pp. 6144–6147, 2011.
[8] V. J. Gokhale, J. Roberts, and M. Rais-Zaden, "Novel uncooled detector based on gallium nitride micromechanical resonators," *Proc. SPIE*, vol. 8353, p. 835319, 2012.
[9] N. I. Landy, S. Sajuyigbe, J. J. Mock, D. R. Smith, and W. J. Padilla, "Perfect metamaterial absorber," *Phys. Rev. Lett.*, vol. 100, p. 207402, 2008.
[10] Y. Ra'di, C. R. Simovski, and S. A. Tretyakov, "Thin perfect absorbers for electromagnetic waves: theory, design, and realizations," *Phys. Rev. Appl.*, vol. 3, p. 037001, 2015.
[11] K. Aydin, V. E. Ferry, R. M. Briggs, and H. A. Atwater, "Broadband polarization-independent resonant light absorption using ultrathin plasmonic super absorbers," *Nat. Commun.*, vol. 2, p. 517, 2011.
[12] G. Dayal and S. A. Ramakrishna, "Design of highly absorbing metamaterials for infrared frequencies," *Opt. Express*, vol. 20, pp. 17503–17508, 2012.
[13] L. Huang, D. R. Chowdhury, S. Ramani, et al., "Experimental demonstration of terahertz metamaterial absorbers with a broad and flat high absorption band," *Opt. Lett.*, vol. 37, pp. 154–156, 2011.
[14] H. Jeong, T. T. Nguyen, and S. Lim, "Meta-dome for broadband radar absorbing structure," *Sci. Rep.*, vol. 8, p. 17893, 2018.
[15] M. K. Hedayati, M. Javaherirahim, B. Mozooni, et al., "Design of a perfect black absorber at visible frequencies using plasmonic metamaterials," *Adv. Mater.*, vol. 23, pp. 5410–5414, 2011.
[16] T. Maier and H. Brückl, "Wavelength-tunable microbolometers with metamaterial absorbers," *Opt. Lett.*, vol. 34, p. 3012, 2009.
[17] M. Diem, T. Koschny, and C. M. Soukoulis, "Wide-angle perfect absorber/thermal emitter in the terahertz regime," *Phys. Rev. B*, vol. 79, p. 33101, 2009.
[18] X. Liu, T. Tyler, T. Starr, A. F. Starr, N. M. Jokerst, and W. J. Padilla, "Taming the blackbody with infrared metamaterials as selective thermal emitters," *Phys. Rev. Lett.*, vol. 107, p. 045901, 2011.
[19] H. A. Atwater and A. Polman, "Plasmonics for improved photovoltaic devices," *Nat. Mater.*, vol. 9, p. 865, 2010.
[20] E. Rephaeli and S. Fan, "Absorber and emitter for solar thermo-photovoltaic systems to achieve efficiency exceeding the Shockley–Queisser limit," *Opt. Express*, vol. 17, p. 15145, 2009.
[21] J. N. Munday and H. A. Atwater, "Large integrated absorption enhancement in plasmonic solar cells by combining metallic gratings and antireflection coatings," *Nano Lett.*, vol. 11, pp. 2195–2201, 2011.
[22] C. Hägglund and S. P. Apell, "Plasmonic near-field absorbers for ultrathin solar cells," *J. Phys. Chem. Lett.*, vol. 3, pp. 1275–1285, 2012.
[23] Y. Huang, Y. Fang, Z. Zhang, L. Zhu, and M. Sun, "Nanowire-supported plasmonic waveguide for remote excitation of surface-enhanced Raman scattering," *Light Sci. Appl.*, vol. 3, p. e199, 2014.
[24] Y. Avitzour, Y. A. Urzhumov, and G. Shvets, "Wide-angle infrared absorber based on a negative-index plasmonic metamaterial," *Phys. Rev. B*, vol. 79, p. 045131, 2009.

[25] S. Ogawa, K. Masuda, Y. Takagawa, and M. Kimata, "Polarization-selective uncooled infrared sensor with asymmetric two-dimensional plasmonic absorber," *Opt. Eng.*, vol. 53, p. 107110, 2014.
[26] Y. Z. Shi, S. Xiong, Y. Zhang, et al., "Sculpting nanoparticle dynamics for single-bacteria-level screening and direct binding-efficiency measurement," *Nat. Commun.*, vol. 9, p. 815, 2018.
[27] Y. Shi, S. Xiong, L. K. Chin, et al., "Sculpting nanoparticle dynamics for single-bacteria-level screening and direct binding-efficiency measurement," *Sci. Adv.*, vol. 4, p. eaao0773, 2018.
[28] M. X. Ren, W. Wu, W. Cai, B. Pi, X. Z. Zhang, and J. J. Xu, "Reconfigurable metasurfaces that enable light polarization control by light," *Light Sci. Appl.*, vol. 6, pp. e16254–5, 2017.
[29] N. Liu, M. Mesch, T. Weiss, M. Hentschel, and H. Giessen, "Infrared perfect absorber and its application as plasmonic sensor," *Nano Lett.*, vol. 10, pp. 2342–2348, 2010.
[30] S. Ogawa, D. Fujisawa, H. Hata, and M. Kimata, "Absorption properties of simply fabricated all-metal mushroom plasmonic metamaterials incorporating tube-shaped posts for multi-color uncooled infrared image sensor applications," *Photonics*, vol. 3, p. 9, 2016.
[31] J. J. Talghader, A. S. Gawarikar, and R. P. Shea, "Spectral selectivity in infrared thermal detection," *Light Sci. Appl.*, vol. 1, p. e24, 2012.
[32] J. Jung, K. Song, J. Choi, et al., "Infrared broadband metasurface absorber for reducing the thermal mass of a microbolometer," *Sci. Rep.*, vol. 7, p. 430, 2017.
[33] T. Maier and H. Brueckl, "Multispectral microbolometers for the midinfrared," *Opt. Lett.*, vol. 35, pp. 3766–3768, 2010.
[34] G. F. P. Sanchez, A. Morales-Acevedo, B. R. Jackson, and C. E. Saavedra, "Thin film bulk acoustic wave resonators for their application in microwave filters," in *2007 4th Int. Conf. Electr. Electron. Eng.*, 2007, pp. 353–356.
[35] T. Kawakubo, "Thin film bulk acoustic wave resonator," *J. Acoust. Soc. Am.*, vol. 118, p. 586, 2005.
[36] V. J. Gokhale and M. Rais-Zadeh, "Uncooled infrared detectors using gallium nitride on silicon micromechanical resonators," *J. Microelectromech. Syst.*, vol. 23, pp. 803–810, 2014.
[37] J. Ibáñez, S. Hernández, E. Alarcón-Lladó, et al., "Far-infrared transmission in GaN, AlN, and AlGaN thin films grown by molecular beam epitaxy," *J. Appl. Phys.*, vol. 104, p. 743, 2008.
[38] J. Kischkat, S. Peters, B. Gruska, et al., "Mid-infrared optical properties of thin films of aluminium oxide, titanium dioxide, silicon dioxide, aluminium nitride, and silicon nitride," *Appl. Opt.*, vol. 51, pp. 6789–6798, 2012.
[39] M. A. Ordal, L. L. Long, R. J. Bell, et al., "Optical properties of the metals Al, Co, Cu, Au, Fe, Pb, Ni, Pd, Pt, Ag, Ti, and W in the infrared and far infrared," *Appl. Opt.*, vol. 22, p. 1099, 1983.
[40] M. A. Ordal, R. J. Bell, R. W. Alexander, Jr, L. L. Long, and M. R. Querry, "Optical properties of fourteen metals in the infrared and far infrared: Al, Co, Cu, Au, Fe, Pb, Mo, Ni, Pd, Pt, Ag, Ti, V, and W," *Appl. Opt.*, vol. 24, p. 4493, 1985.
[41] J. Hao, J. Wang, X. Liu, W. J. Padilla, L. Zhou, and M. Qiu, "High performance optical absorber based on a plasmonic metamaterial," *Appl. Phys. Lett.*, vol. 96, p. 251104, 2010.
[42] Y. Shang, X. Ye, M. Wang, P. Song, and J. Feng, "Design, fabrication, and characterization of a polymer-based MEMS uncooled infrared focal plane array," *J. Microelectromech. Syst.*, vol. 24, pp. 1132–1141, 2015.

Supplementary Material: The online version of this article offers supplementary material (https://doi.org/10.1515/nanoph-2020-0607).